Molecular and Cellular Biochemistry (2023) 478:229–240
https://doi.org/10.1007/s11010-022-04473-6

Investigating microRNAs in diabetic cardiomyopathy as tools for early detection and therapeutics

Priyanka Mathur[1] · **Vibha Rani**[1]

Received: 19 December 2021 / Accepted: 4 May 2022 / Published online: 2 July 2022

Abstract

To profile microRNAs population of glucose-induced cardiomyoblast cell line and identify the differentially expressed microRNAs and their role under pre-diabetes and diabetes condition in vitro. Rat fetal ventricular cardiomyoblast cell line H9c2 was treated with D-glucose to mimic pre-diabetic, diabetic, and high-glucose conditions. Alteration in cellular, nuclear morphology, and change in ROS generation was analyzed through fluorescent staining. Small RNA sequencing was performed using Illumina NextSeq 550 sequencer and was validated using stem–loop qRT-PCR. A large number (~ 100) differential miRNAs were detected in each treated samples as compared to control; however, a similar expression pattern was observed between pre-diabetes and diabetes conditions with the exception for miR-429, miR-101b-5p, miR-503-3p, miR-384-5p, miR-412-5p, miR-672-5p, and miR-532-3p. Functional annotation of differential expressed target genes revealed their involvement in significantly enriched key pathways associated with diabetic cardiomyopathy. For the first time, we report the differential expression of miRNAs (miR-1249, miR-3596d, miR- 3586-3p, miR-7b-3p, miR-191, miR-330-3p, miR-328a, let7i-5p, miR-146-3p, miR-26a-3p) in diabetes-induced cardiac cells. Hyperglycemia threatens the cell homeostasis by dysregulation of miRNAs that begins at a glucose level 10 mM and remains undetected. Analysis of differential expressed miRNAs in pre-diabetes and diabetes conditions and their role in regulatory mechanisms of diabetic cardiomyopathy holds high potential in the direction of using miRNAs as minimally invasive diagnostic and therapeutic tools.

Keywords Diabetic cardiomyopathy · MicroRNAs · Pre-diabetes · Small RNA sequencing · Biomarkers · Therapeutics

Introduction

Affecting nearly 463 million people worldwide, diabetes features among the top causes of mortality and morbidity around the globe [1]. World Health Organization (WHO) has predicted a two-time increase in the number of deaths due to diabetes between 2005 and 2030, which at present is expected to be much higher considering the global prevalence of the COVID-19 pandemic since 2019 [2]. Diabetes majorly contributes to the onset and pathogenesis of life-threatening diseases including cardiomyopathy leading to cardiac failure [3]. Cardiac failure in diabetic patients was first recognized in 1876; however, the term diabetic cardiomyopathy (DCM) was introduced much later in 1972 by Rubler et al. [4, 5]. Till now, diabetic cardiomyopathy lacks a consistent and universally accepted definition with the AHA (American Heart Association), ESC (European Society of Cardiology), and ADA (American Diabetes Association) yet to define DCM. In general, DCM is defined as cardiac dysfunction resulting from structural, functional, and metabolic alterations independent of coronary artery diseases, such as hypertension, valvular diseases, and atherosclerosis [6]. Diabetes poses a tenfold risk factor in developing cardiomyopathy and heart failure which is a major concern considering the pandemic nature of Type 2 diabetes mellitus (T2DM) [7]. Previous studies suggest that besides T2DM, pre-diabetes (which lacks a clear symptom and mostly remains undiagnosed) independently increases the risk of cardiomyopathy [8–10]. Therefore, molecular mechanisms and pathways involved in the pre-diabetes phase, as compared to diabetes and high-glucose-induced cardiac stress, must be studied for early detection and planning advanced therapeutic strategies.

✉ Vibha Rani
vibha.rani@jiit.ac.in

[1] Transcriptome Laboratory, Centre for Emerging Diseases, Department of Biotechnology, Jaypee Institute of Information Technology, A-10, Sector-62, Noida, Uttar Pradesh 210309, India

MicroRNAs (miRNAs) have emerged as a critical regulator of entire networks of transcripts through post-transcriptional modifications. They are small (~ 22 nucleotides), non-coding RNAs that possess several attributes including binding to the 3'-untranslated region (3'UTR) of their target mRNA, binding to the double-stranded DNA at a specific site, and interaction with complementary miRNAs to mediate their function and regulate gene expression [11–13]. In the heart, miRNAs maintain cell homeostasis as well as pathological conditions, including hypertrophy, contractility, and cardiomyopathies [14]. Previously, several studies have reported a considerable number of miRNAs to be dysregulated under diabetic conditions in in vitro, in vivo, and clinical cardiac samples [15–21]. However, the in-depth miRNAs sequencing of cardiac muscle cells under often undetected pre-diabetic, diabetic, and high-glucose conditions is still lacking. Our previous study has shown deleterious effect of glucose stress on H9C2 cardiomyoblast through evaluation of oxidative stress, assessment of anti-oxidant enzymes activity, change in cell and nuclear morphology, and estimation of collagen content [22]. The present study aims to profile the miRNAs landscape of the cardiomyoblast cell line (differentiates into cardiomyocytes) treated with different concentrations of D-glucose to mimic the pre-diabetic (10 mM), diabetic (25 mM), and high-glucose (50 mM) conditions using high-throughput small RNA sequencing. Further, we used complementary bioinformatics to identify the potential mRNA targets and their role in the glucose-induced cardiac stress.

Materials and methods

All the reagents and chemicals were purchased from Sigma-Aldrich (USA) unless or otherwise mentioned.

Cell culture and sample preparation

H9C2, an immortal cardiomyoblast cell line isolated from the embryonic rat heart tissue, was obtained from the National Center for Cell Science (NCCS), Pune, India. The cells were cultured in Dulbecco's modified Eagle medium (DMEM) supplemented with 10% fetal bovine serum (FBS), 100 U per mL penicillin, and 100 µg per mL streptomycin in a humidified incubator under a normal culture condition (5% CO_2, 37 °C). Cells were routinely passaged at a split ratio of 1:3. Once nearly 70% confluence was reached, the cells were treated with D-glucose at the concentration of 10 mM (G10), 25 mM (G25), and 50 mM (G50) with media supplemented with Insulin-Transferrin-Selenium (ITS) and devoid of FBS. After 48 h of incubation, the cells were thoroughly washed with cold PBS and extracted for RNA isolation.

Cell and nuclear morphological analysis of glucose-induced H9C2 cells

Four sets of H9C2 were cultured for 24 h out of which three sets (here after referred as G10, G25, and G50) were induced with D-glucose (10 mM, 25 mM, 50 mM, respectively) dissolved in incomplete media containing 5X Insulin-Transferrin-Selenium (ITS) and kept at 37 °C, 5% CO_2 for 48 h. To study cell morphology, cells were fixed using 100% methanol followed by incubation at − 20 °C for 30 min. Cells were treated with Giemsa stain for 20 min at room temperature and were visualized under an inverted microscope at 40× magnification and cell size was quantified using NIH ImageJ software. To study nuclear morphology, both control and treated cells were stained using DAPI (50 ng/ml) prepared by dissolving the stain in Tris–HCl (10 mM, pH 7.4), EDTA (10 mM, pH 8), and NaCl (100 mM). Alteration in nuclear morphology was visualized at 40× magnification and the fluorescence intensity was measured at an excitation and emission wavelength of 372 and 456 nm, respectively.

Estimation of cellular ROS generation

The ROS generated by control and D-glucose-treated H9C2 cells was estimated through DCFH-DA staining. Cells were cultured, treated, and fixed as mentioned previously. Cells were stained using 5 µM of 2′,7′-dichlorofluorescin diacetate (DCFH-DA) followed by incubation for 30 min at room temperature in dark. The cells were visualized at 40× magnification and the fluorescence intensity was measured at excitation and emission wavelength of 490 and 520 nm.

RNA isolation and quality control

D-glucose-treated and untreated cells were homogenized with TOMY Micro smasher_MS100 (USA) and lysed with 300 µl of Lysis/Binding Buffer (Qiagen). Homogenate additive was added to the lysate at one-tenth of the lysate volume followed by the addition of acid Phenol–Chloroform. After a brief vortex and centrifugation, the upper aqueous phase was aspirated into a new vial. The aqueous phase was mixed with 1.25 volumes of 100% ethanol and loaded onto a filter cartridge. The remaining steps of the purification were followed as per the manufacturer's guidelines including on-column DNase treatment (Qiagen). RNA was eluted in 25 µl of Nuclease-free water (Ambion). The concentration and purity of the RNA extracted were evaluated using the Nanodrop Spectrophotometer (Thermo Scientific). The RNA content (ng/µl) for each sample is as follows (G10: 42.4; G25: 80.3; G50: 16; and Control: 118.8). The integrity of the extracted

RNA was analyzed on the Bioanalyzer (Agilent) and the RIN value for each sample was found to be 7 or higher.

Small RNA library preparation and sequencing

Small RNA sequencing libraries were prepared using the QIAseq miRNA Library Kit protocol (Qiagen) at Genotypic Technology Pvt. Ltd., Bangalore, India. Briefly, 100 ng of Qubit-quantified total RNA was used as starting material. 3′ adapters were ligated to the specific 3′ OH group of microRNAs followed by ligation of 5′ adapter. Adapter-ligated fragment was reverse transcribed with Unique Molecular Index (UMI) assignment by priming with reverse transcription primers. cDNA thus synthesized was enriched and barcoded in a single step by PCR amplification (17 cycles). The 3′ and 5′ adapters used in the prep were as follows: 5′ GTTCAGAGTTCTACAGTCCGACGATC; Index Adapter: 5′ AACTGTAGGCACCATCAAT. The Illumina-compatible sequencing libraries were quantified by Qubit fluorometer (Thermo Fisher Scientific) and the fragment size distribution of the libraries was analyzed on Agilent 2200 TapeStation. Single-end sequencing was carried out for 75 cycles on Illumina NextSeq 550 sequencer using High Output flow cells and reagents, following manufacturer's instructions.

Data processing and analysis

The raw data were processed by srna-workbenchV3.0_ALPHA which was used to trim 3′ adapter and performed length filtering (minimum length 16 bp and maximum 40 bp). The low quality and contaminated reads were removed on the following criteria to obtain final clean reads: (a) Elimination of low-quality reads (< q30), (b) Elimination of 3′ adapters, (c) Elimination of reads < 16 bp and > 40 bp, and (d) Elimination of reads matching to other non-coding RNAs (rRNA, tRNA, snRNA, and snoRNAs). The filtered reads were mapped to the Rattus norvegicus genome using Bowtie. These reads were further mapped to a non-coding RNA database which is useful to exclude the other RNAs, such as rRNA, tRNA, and snoRNAs. The unmapped reads which should be only small RNAs were used for the classification of known and novel miRNAs and target prediction.

MiRNAs identification and expression analysis

The final clean reads were made unique and hence read count profile was generated. Further, a homology search was performed for these miRNAs against Rattus norvegicus miRNA sequences which were retrieved from miRbase-22 using NCBI-blast-2.2.30 with an e-value of e-4 and non-gapped aligned. Sequences that have no homology with known miRNAs were extracted and considered for the prediction of potential novel miRNAs. Firstly, the sequences were aligned to the reference genome using bowtie. The aligned sequences were used for novel miRNAs prediction using Mireap_0.22b. To perform differential expression analysis, read counts across all the miRNAs were generated by taking the count of reads aligning to a particular miRNA. Differential expression (DE) was calculated using the DESeq tool through normalizing the read count by dividing with size factor (Read count/Geometric Mean). Mean-normalized read counts of the samples in a given condition were used for differential gene expression calculation and heatmap generation. To understand the regulation of expression between the samples, log2fold of 1 was used as a cut-off. MiRNAs > 1 were considered as "UP"-regulated, miRNAs < − 1 were considered as "DOWN," and those between 1 and − 1 were flagged as "NEUTRAL."

Stem–loop qRT-PCR

RNA isolation was performed from the treated (G10, G25, and G50) and a control set of H9C2 culture as described previously. Stem–loop primers were synthesized for miR-532-3p and miR-672-5p as mentioned in our previous study (supplementary table) [11]. The stem–loop reverse transcription was performed using the RevertAid First-Strand cDNA Synthesis Kit (Thermo Scientific, USA) as per the manufacturer's protocol. A reaction mixture of 10 µL was prepared using 1 µL RNA (~ 200 ng), 1 µL miRNA stem–loop primer (1 µM), 1 µL U6 RT primer (1 µM), 0.5 µL RiboLock (20 U/µL), 2 µL buffer, 1 µL dNTP mix (10 mM), 0.5 µL reverse transcriptase enzyme (200 U/µL), and 3 µL nuclease-free water. The reverse transcription reaction was carried out at 25 °C for 5 min followed by incubation at 42 °C for 60 min and termination by heating at 70 °C for 5 min. SYBR green fluorescence quantitative PCR reagent kit (Thermo Fischer Scientific, USA) and Piko-Real Time 96 (Thermo Fischer Scientific, USA) was used for RT-PCR. The reaction mixture of 10 µL was prepared in Piko 96-well plate using 5 µL SYBR green PCR Master Mix, 0.5 µL forward and reverse primers each (1 µM), 1 µL cDNA product, and 3 µL nuclease-free water. The PCR conditions used were as follows: initial denaturation at 95 °C for 30 s, followed by 40 cycles of 95 °C for 15 s, and 55 °C for 30 s. Each reaction was performed in triplicates and the relative expression of miRNA was calculated using $2^{-\Delta\Delta Cq}$ after normalization to U6 snRNA.

Target Prediction and annotation

The miRNAs with copy number ≥ 5 were considered for target prediction. These miRNA sequences were used as input along with reference cDNA sequences to the Miranda tool. Gene Ontology annotation was performed by PANTHER

14.1 database and the pathway enrichment analysis was performed using DAVID 6.8

Statistical analyses

Each experiment was conducted thrice and data were expressed as means ± SEM. A two-tailed unpaired Student's *t* test was used for statistical comparison of the data between control and treatment or between two treatment groups. From DAVID database, Fisher's exact test was used to determine the probability that the GO terms assigned to the dataset are due to chance alone, and p values < 0.05 and enrichment score of > 1.5 were considered to be statistically significant.

Results

Microscopic analysis of glucose-induced H9C2 cells

Post-24 h of glucose treatment, H9C2 cells were subjected to Giemsa staining (for cell morphology), DAPI staining (for nuclear morphology), and DCFH (for ROS estimation). We observed that at 10 mM, glucose initiates the change in cell morphology but limited to very few number of cells and does not cause any significant change in the cell as well as nuclear morphology. In addition, it also did not elicit a significant change in ROS generation as compared to untreated cell. However, at 25 mM and 50 mM, we observed a significant difference in cell size of H9C2 indicating induction of hypertrophy. We also observed high ROS generation in sample G25 and a significant difference in G50. Although, through DAPI staining we did not observe a change in the fluorescent intensity between treated and untreated samples, we observed a greater number of condensed chromatin (black arrow), fragmented nuclei (yellow arrow), and distorted nuclei of varying shape and size (red arrow) (Fig. 1).

High-throughput sequencing

To determine the effect of D-glucose on the cardiomyoblast miRNAs, four small RNA libraries (one untreated and three treated including 10 mM, 25 mM, and 50 mM) were generated. After performing high-throughput sequencing, a total of 71.2 million raw reads and 3.0 million high-quality reads were obtained from all the samples. The distribution of reads count and the number of known as well as novel miRNAs for each sample are provided in Table 1. After alignment, RNAs were classified into different categories, such as rRNA, tRNA, snRNA, snoRNA, known miRNA, and novel miRNA. More than 60% of the reads were found to align

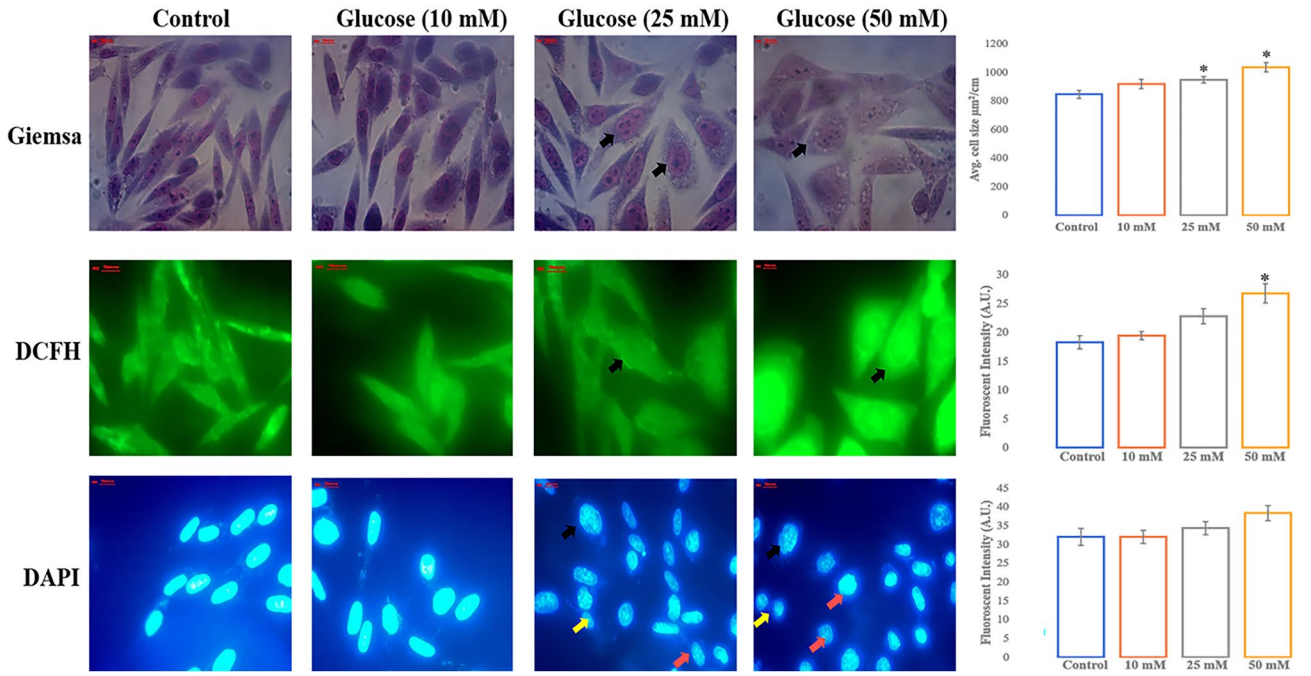

Fig. 1 Cellular and nuclear morphological alterations in D-glucose-induced H9C2 cells. Top row indicates the increase in cell size in G25 (approx. 900 µm/cm^2) and G50 (approx. 1000 µm/cm^2). Middle row indicates the increase in ROS generation in G25 (Fluorescent intensity approx. 20 A.U.) and G50 (Fluorescent intensity approx. 25 A.U.). Bottom row indicates the high number of nuclei with fragmented nuclei (yellow arrow), condensed chromatin (red arrow), and distorted nuclei of varying shape and size (black arrow). (*$p < 0.05$ vs untreated)

Table 1 Representation of high-throughput sequencing with total of 71.2 million raw reads, along with distribution of reads count and the number of known as well as novel miRNAs for each sample

Sequencing statistics	Untreated	Glucose (10 mM)	Glucose (25 mM)	Glucose (50 mM)
Total raw reads	14,094,628	17,996,201	19,045,124	20,157,742
Total number of reads after quality filtering	659,709	866,393	630,543	910,684
Total reads aligned to the genome (Rattus Noverglicus)	403,529	529,260	396,444	557,791
Percentage of reads mapped to genome (Rattus Norvegicus)	61.17	61.09	62.87	61.25
Percentage of reads aligned to non-coding RNAs	17.66	18.45	19.29	21.79
Total reads aligned to mirBase database	8892	10,998	10,548	10,149
Known miRNAs detected	373	401	379	395
Known miRNAs detected with abudance ≥ 50	187	204	198	190
Known miRNAs detected with abudance ≥ 10	257	276	258	269
Putative novel miRNAs detected	67	59	57	87
Putative novel miRNAs detected with abudnace ≥ 10	34	29	33	41

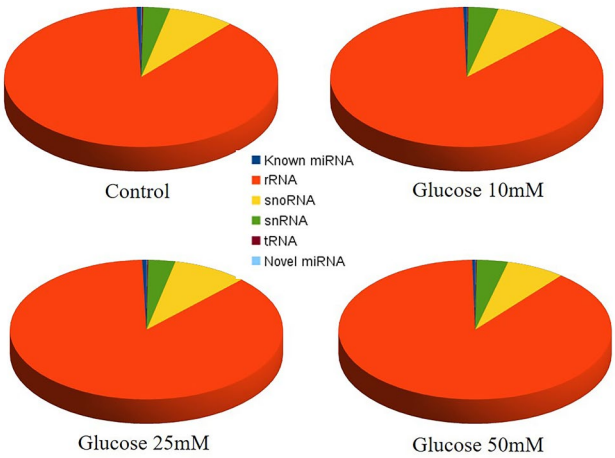

Fig. 2 Pie charts indicating the distribution of RNA and small non-coding RNAs across all the samples

with the Rattus Norvegicus genome out of which nearly 19% aligned with non-coding RNAs (Fig. 2).

Identification of miRNA in D-glucose-induced H9C2 cells

Through high-throughput sequencing, we have identified more than 350 miRNAs in each H9C2 sample out of which more than 180 miRNAs were detected with abundance ≥ 50 (Table 1). A deep examination of the small RNA sequences revealed that the size of most miRNAs ranged between 21 and 24 nucleotides with the maximum number of miRNAs of 22 nucleotide size (Fig. 3). Further, chromosomal distribution of miRNAs origin was studied and it was observed that the maximum number of miRNAs was expressed from chromosome numbers X, 1, and 10 (Fig. 4). To identify the differential expressed miRNAs in treated samples as compared to control, a volcano plot-based filtering was performed (Fig. 5). We observed that as compared to control, 47 miRNAs were upregulated and 47 were downregulated in G10, 50 miRNAs were upregulated and 62 miRNAs downregulated in G25, while 56 miRNAs were upregulated and 49 miRNAs as downregulated in G50 (log2 Fold Change > 1 or log2 Fold Change < -1with FDR < 0.05). To list the top 20 up/down-regulated miRNAs and identify their expression difference heatmaps were generated for each set of differentially expressed miRNAs (Supplementary Fig S1–S3). In the top 20 up/down miRNAs of G10, 27 were intergenic (15 upregulated and 12 downregulated) and 13 were intronic (4 upregulated and 9 downregulated). In G25, 27 were intergenic (14 upregulated and 13 downregulated) and 12 were intronic (4 upregulated and 8 downregulated). Lastly in G50, 22 were intergenic (11 upregulated and 11 downregulated) and 18 were intronic (10 upregulated and 8 downregulated) as compared to control. A comparative heatmap analysis of all the treated samples revealed a similar trend in expression across all the treated samples as compared to control (Fig. 6). The common upregulated miRNAs detected in all the samples include miR-1249, miR-330-3p, miR-3473, miR-143-3p, miR-132-5p, miR-223-3p, miR-328a-3p, miR-29c-3p, miR-16-5p,miR-628,let-7i-5p, miR-146b-3p, miR-3596d, and miR-3586-3p, whereas the downregulated miRNAs include mir-7b-3p, mir-542, mir-9a-5p, mir-222-5p, mir-191b, miR-26a-3p, miR-30d-3p, miR-142-3p, miR-652-5p, miR-126a-3p, miR-29c-3p, miR-328a-3p, miR-345-3p, miR-148a-3p, miR-15a-5p, and miR-15b-5p. These miRNAs were considered for target prediction and their functional annotation. We also detected very few miRNAs depicting contrasting expression in G10 and as compared to G25 and G50. They include miR-429, miR-101b-5p, miR-503-3p, miR-384-5p, miR-412-5p, miR-672-5p (downregulated in

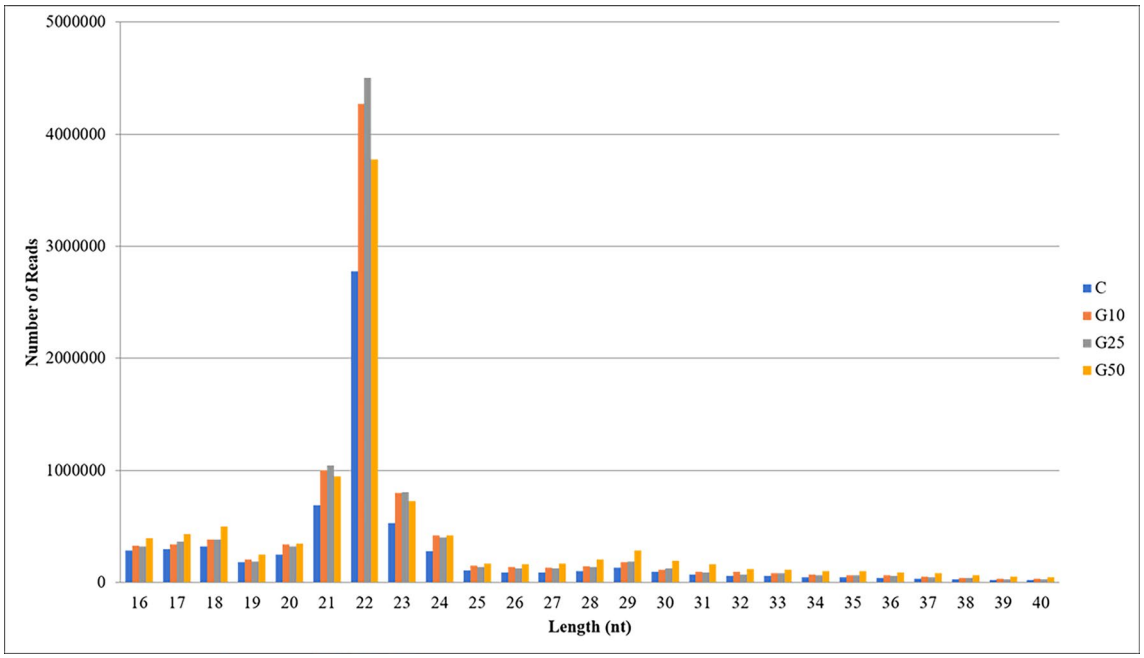

Fig. 3 Bar graph indicating the length distribution of RNA-seq reads. Maximum miRNAs were observed to be of 22 nucleotide length

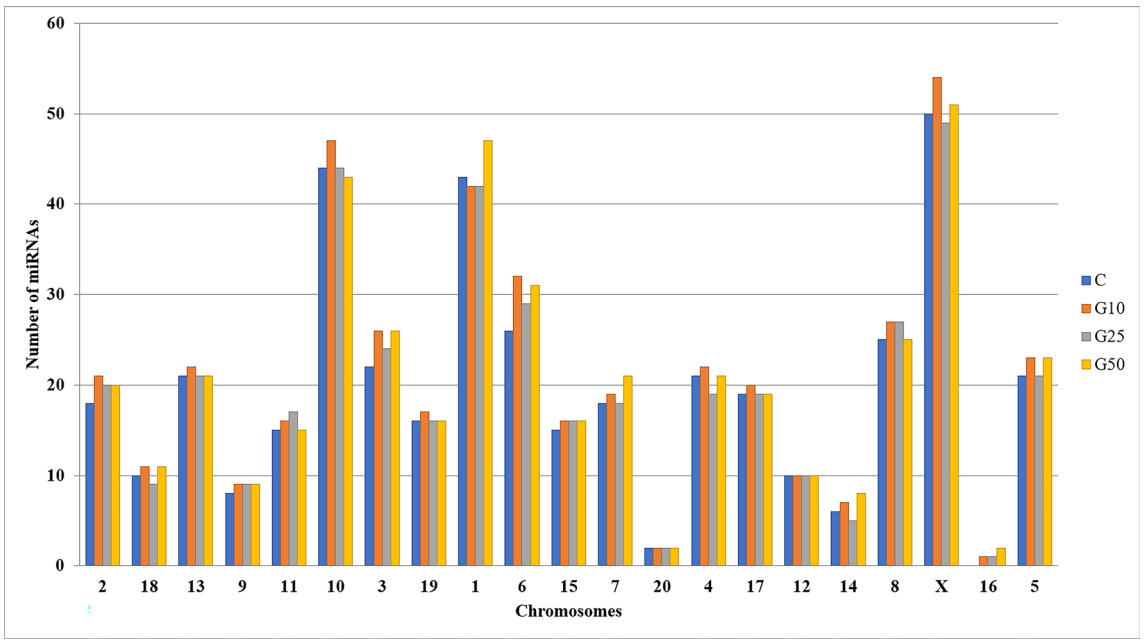

Fig. 4 Bar graph indicating the chromosomal distribution of miRNAs in *Rattus norvegicus* genome

G10 and upregulated in G25 and G50), and miR-532-3p (upregulated in G10 and downregulated in G25 and G50).

Potential target mRNA/gene prediction and their functional annotation

Potential target prediction for all the miRNAs identified in control as well as treated samples was performed using Miranda and miRNA hits having minimum free energy ≤ -25 were considered for further analysis. In total, 18,741, 19,128,

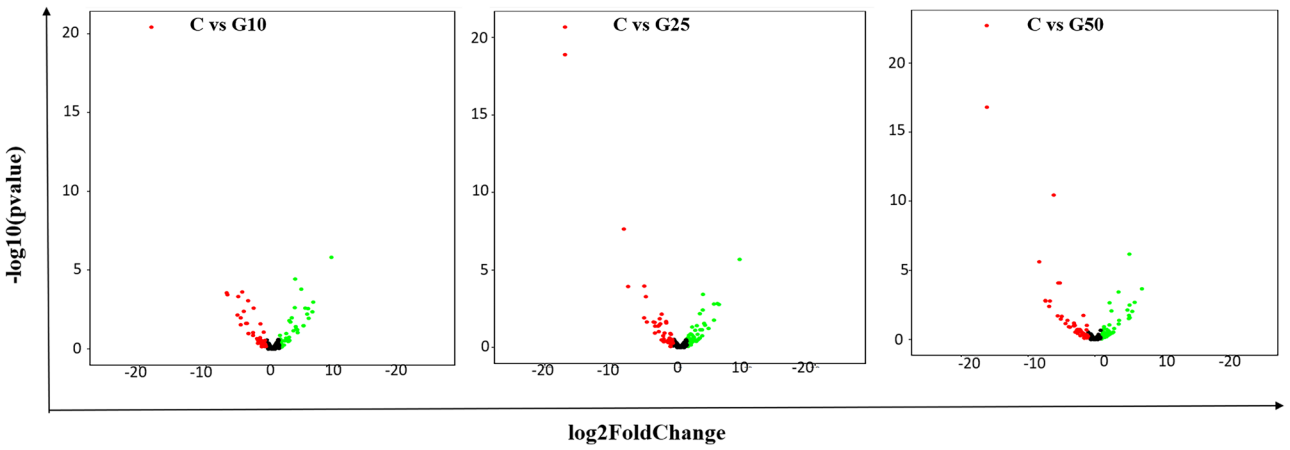

Fig. 5 Volcano plot analysis of differential expressed miRNAs. The expression differences in miRNAs between control and G10, control and G25, and control and G50 was plotted on the x-axis and FDR significance was plotted on the Y-axis (−log10 scale). The black dots represent no change in expression, the red dots represent log fold change of > 1 and FDR < 0.05, and green dots represent log fold change < 1 and FDR < 0.05

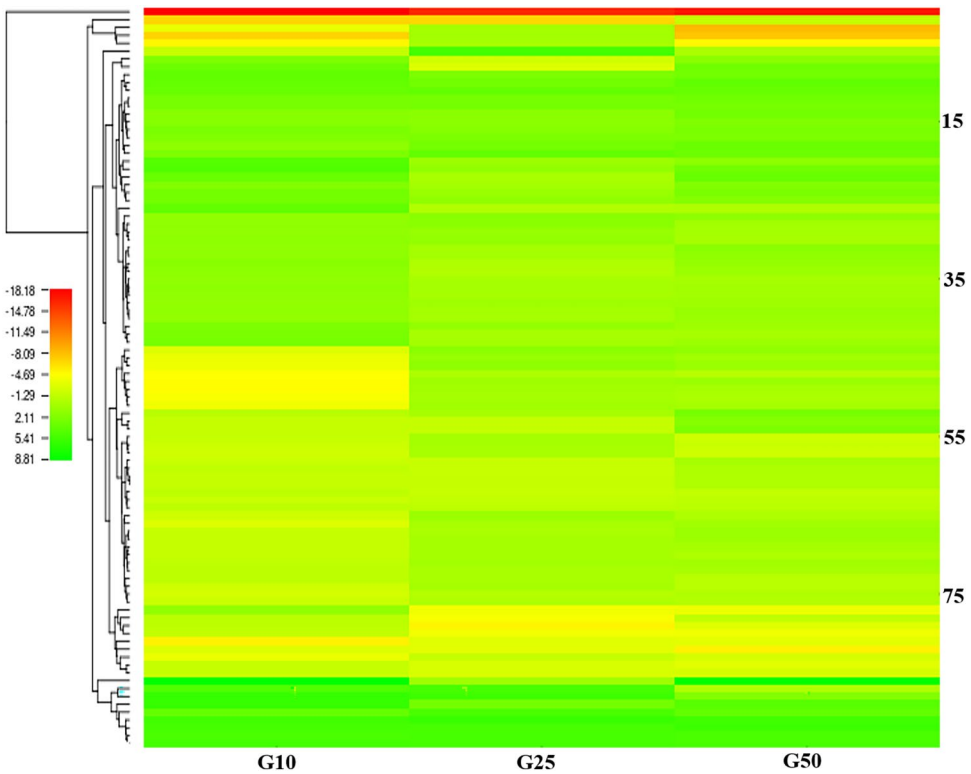

Fig. 6 Heatmap indicating the miRNAs expression pattern across all the treated samples. Green color indicates upregulation, whereas red color indicates downregulation of miRNAs

18,307, and 18,993 unique targets were predicted for control, G10, G20, and G50 samples, respectively. Target genes of differentially expressed miRNAs identified in all the treated samples were selected and Gene Ontology was performed to understand their biological meaning. Analysis through PANTHER database revealed that in all the treated samples similar percentage of target genes of up- and downregulated miRNAs were represented in all the three categories: cellular component (cellular anatomical entity: 50%, protein-containing complex: 13%, and intracellular: 37%), biological process (cellular process: 30%, biological regulation: 18%, metabolic process: 17% and signaling: 7% others: 28%), and molecular function (binding: 40%, catalytic activity: 30%, molecular function regulator: 18%, transporter activity: 8%). The functional enrichment analysis through the DAVID database revealed the top 20 gene target-enriched GO terms and KEGG pathways with *p*

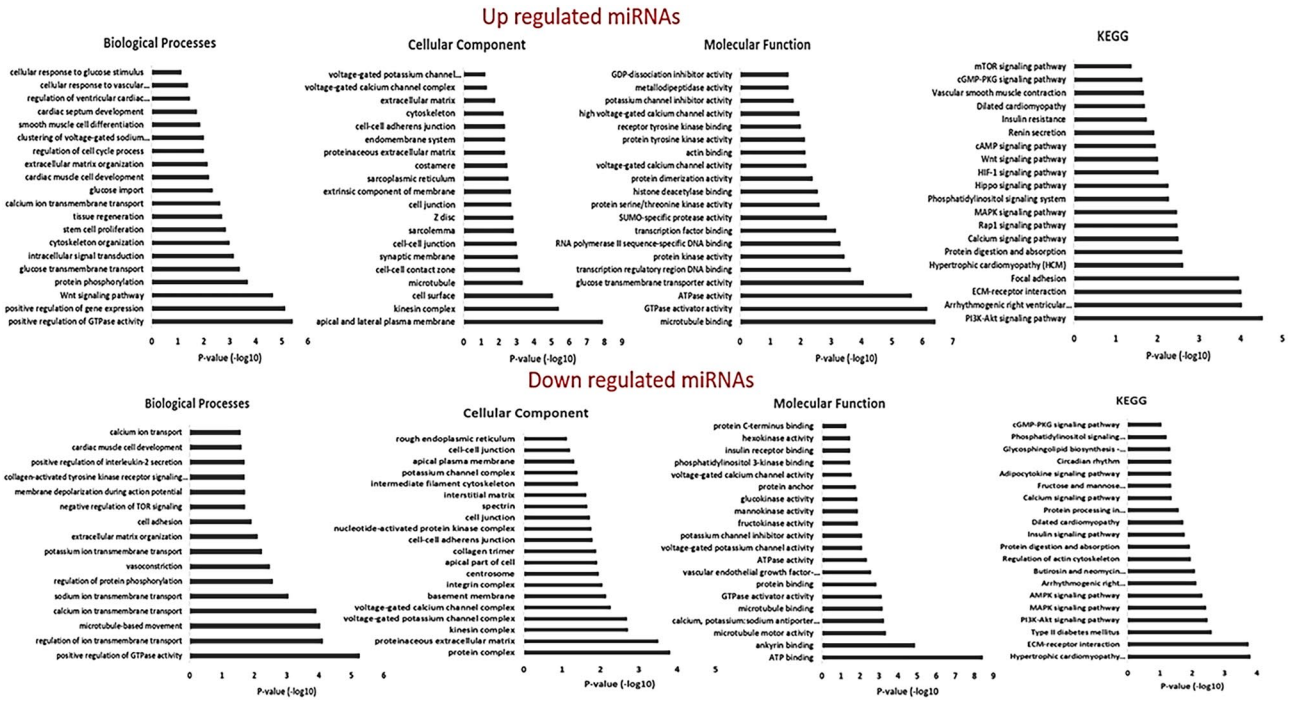

Fig. 7 Gene ontology (GO terms: Biological processes, Cellular component, Molecular Function) and KEGG analysis of differential expressed miRNAs target genes

values < 0.05and enrichment score of > 1.5 (Fig. 7). The target genes of upregulated miRNAs were significantly enriched in KEGG pathways, including PI3K-Akt signaling pathway (*p* value: 3.00E-05, Fold Enrichment: 1.9), arrhythmogenic right ventricular cardiomyopathy (*p* value: 1.10E-04, Fold Enrichment: 3.2), ECM–receptor interaction (*p* value: 9.50E-05, Fold Enrichment: 2.8), and hypertrophic cardiomyopathy (*p* value: 2.40E-03, Fold Enrichment: 2.5). Likewise, the target genes of downregulated miRNAs were significantly enriched in KEGG pathways, including hypertrophic cardiomyopathy (*p* value: 1.60E-04, Fold Enrichment: 2.9), ECM–receptor interaction (*p* value: 1.80E-04, Fold Enrichment: 2.8), type II diabetes mellitus (*p* value: 3.70E-03, Fold Enrichment: 2.9), as well as insulin signaling pathway (*p* value: 1.20E-02, Fold Enrichment: 1.9).

Validation of miRNA expression by stem–loop qRT-PCR

The expression validation of two miRNAs (namely, miR-532-3p and miR-672-5p) was performed using stem–loop qRT-PCR. These miRNAs were selected based upon our in silico analysis which reveals (a) differential expression between G10 and other treatment groups (G25 and G50) and (b) targets multiple critical pathways including hypertrophic cardiomyopathy, insulin secretion, and adrenergic signaling in cardiomyocytes (Fig. 8). The results obtained from qRT-PCR were in agreement with the NGS analysis (Fig. 9).

Discussion

MiRNAs, due to their fundamental role in regulating gene expression, are increasingly recognized as therapeutics as well as diagnostic tool for a number of diseases. Although, the association of several miRNAs including miR-1, miR-9, miR-20, miR-21, miR-29, miR-30, miR-34, miR-125, miR-133, miR-143, miR-146, miR-150, miR-155, miR-181, miR-195, miR-199, miR-208, miR-144, miR-206, miR-207, miR-212, miR-221, miR-320, miR-373, miR-378, and miR-499 has been well studied in diabetes and cardiovascular pathologies [21, 23–25]. An in-depth

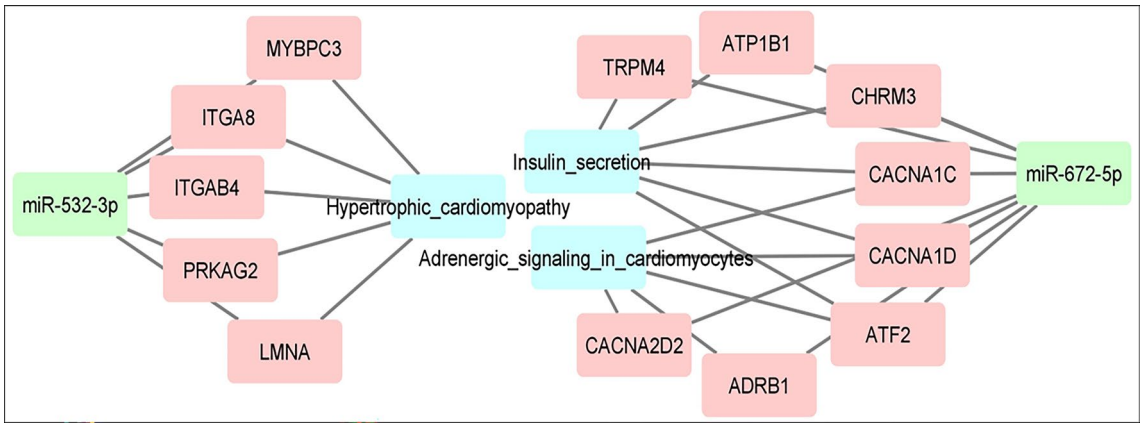

Fig. 8 An interaction network between the miRNAs (miR-532-3p and miR-672-5p), their potential target genes, and significantly enriched and KEEG pathways

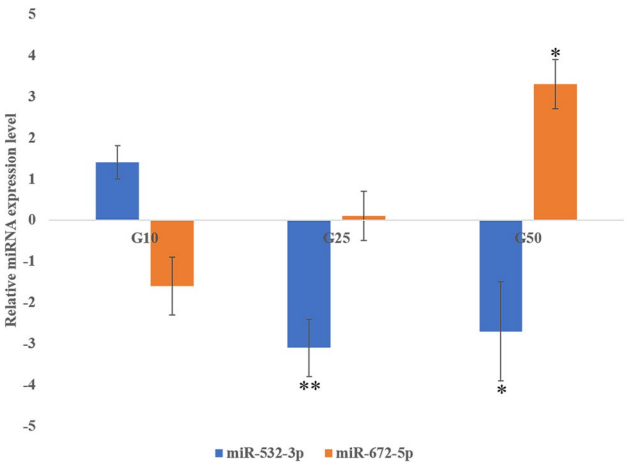

Fig. 9 Stem–loop qRT-PCR validation of miRNAs. The y-axis indicates the fold change expression of miRNAs in treated samples as compared to control ($y=1$). (*$p<0.05$ vs untreated, (**$p<0.01$ vs untreated)

miRNAs profiling representing the entire miRNAs landscape of diabetes-induced cardiac cells is still lacking. In addition, it is also not clear whether the pre-diabetes conditions which are known to increase cardiovascular risks influence miRNAs expression to the extent diabetes conditions does. Toward this, we have performed genome-wide small RNAs sequencing to reveal the miRNAs expression pattern in cardiomyoblast cells induced with pre-diabetic, diabetic, and high-glucose dose. H9C2 cardiomyoblast cells were used as in vitro diabetic model as they are a well-established model for molecular studies on cardiac hypertrophy and related traits [26]. The D-glucose dose of 10 mM, 25 mM, and 50 mM was selected based upon the parameters defined by ADA for pre-diabetes and previous studies including our research elaborating induction of diabetic conditions in H9C2 cell culture [22, 27–29].

As previously mentioned, we have identified a substantial number of differentially expressed miRNAs in all the treated samples in comparison to untreated sample. Except for miR-429, miR-101b-5p, miR-503-3p, miR-384-5p, miR-412-5p, miR-532-3p, and miR-672-5p the top 20 upregulated and downregulated miRNAs depicted a similar expression pattern in cells treated with different concentrations of glucose as compared to untreated cells. This indicates that even though pre-diabetes (10 mM) does not alter the cardiac cell morphology or induces a significant change in ROS generation as indicated through microscopic analysis, it imposes a drastic change in the expression of miRNAs which remains unaltered even at extreme hyperglycemic conditions as compared to untreated cells. Except for miR-3586-3p and miR-3596d, all the common up- and downregulated miRNAs observed between G10, G25, and G50 has been reported in circulation profile of diabetes subjects; however, only a few of them have been reported in cardiac cells or tissue under glucose mediated stress [24, 30–32]. For instance, there are pre-clinic reports which are in agreement with our observation that miR-132-5p, miR-223, and miR-16 remain upregulated, while mir-542, miR-9, miR-222, miR-126a, miR-29c, miR-345, miR-142-3p, miR-148a, and miR-15a/b remain downregulated in DCM [33–42]. On the contrary to our findings, there are reports which suggest that miRNAs including miR-3473, miR-143-3p, and miR-29c remain downregulated, while miR-30d remains upregulated in DCM [30, 43, 44]. The reason for difference in expression of few miRNAs may be due to the different source of sampling or different source of metabolic dysregulation. Nevertheless, appearance of these miRNAs in different diabetic cardiomyopathy model through various sequencing platforms indicates their importance in cardiac cell dysfunction due to diabetes. To the best of our knowledge, we have identified several differentially expressed

conserved miRNAs (miR-1249, miR-3596d, miR-3586-3p, mir-7b-3p, mir-191b) that have not been reported in any cardiovascular complication including DCM along with miRNAs (miR-330-3p, miR-328a, let-7i-5p, miR-146b-3p, miR-26a-3p) that have been studied in valve calcification, adverse cardiac remodeling, and myocardial ischemia, but still unreported in DCM.

Thus, to reveal the biological function of all the common differential miRNAs we predicted potential target genes and performed their functional annotation using the most sensitive and reliable bioinformatic tools, such as MiRanda and DAVID [45]. We observed that the most enriched GO terms under biological process were positive regulation of GTPase activity and regulation of ion transmembrane transport, including calcium ion, wnt signaling and glucose transmembrane transport. Likewise, under molecular function the most enriched terms were ATP binding, GTPase activator activity, and glucose transporter activity, while under cellular component they were protein complexes particularly related to plasma membrane and extracellular matrix. It suggests that glucose induces a change in the expression in a large number of miRNAs that in turn target the genes involved in G-protein activation which is majorly linked with the pathogenesis of DCM through impaired calcium ion signaling, GLUT transporters, and ion transport [46–49]. In particular, the target genes of downregulated miRNAs were found to be involved in regulation of sodium and calcium ion transport. These ions are the most osmotically active species in cardiac myocytes and the abundance of ROS in H9C2 cells as confirmed through DCFH-assay might have a role in miRNAs dysregulation as indicated previously [50, 51]. Further KEGG analysis established that the potential target genes of both upregulated and downregulated miRNAs were enriched in pathways that directly regulate the pathogenesis of DCM, including PI3K-AKT signaling pathway, hypertrophic cardiomyopathy, ECM receptor interaction, type 2 diabetes mellitus, and MAPK signaling [11, 52].

On one hand our analysis revealed a list of miRNAs depicting similar expression upon different doses of glucose induction, and on the other hand we also looked into two miRNAs, namely rno-miR-532-3p and rno-miR-672-5p depicting contrasting expression between G10 as compared to G25 and G50. For rno-miR-532-3p, the fold difference observed in G10, G25, and G50 through NGS was 1.0, − 3.8, and − 3.7, while for rno-miR-672-5p it was − 1.0, 0.01, and 2.5, respectively. Through qRT-PCR, the fold difference observed for rno-miR-532-3p was 1.4, − 3.1, and − 2.7, while for rno-miR-672-5p it was -1.6, 0.1, and 3.32.8 in G10, G25, and G50, respectively. Although the pattern in the expression analysis through qRT-PCR and NGS appeared to correlate with each other, yet it was not precise. It could be due to (a) difference in the platforms for analyzing the miRNAs expression, (b) difference in the methodology used for normalization, and (c) biological difference due to the use of independent samples in qRT-PCR and NGS. Recently, in isoproterenol-treated H9C2 cells, miR-532-3p was reported to be downregulated and its overexpression was found to reduce the cell apoptosis [53]. On the contrary, in animal model of type 2 diabetes and left ventricle samples of diabetic patients, miR-532-3p was reported to be upregulated and its suppression was found to reduce high-glucose-induced apoptosis [54]. We found miR-532-3p to be upregulated in pre-diabetic condition and downregulated in high-glucose conditions with its target genes (MYBPC2, ITGA8, ITGAB4, PRKAG2, and LMNA) enriched in KEGG pathway called hypertrophic cardiomyopathy (p value: 0.03; fold enrichment: 4.2). It suggests that miR-532-3p holds high potential to regulate cardiac hypertrophy and cell death and may also serve as biomarker for pre-diabetes as it has been established in plasma profiles of colorectal cancer patients [55]. Likewise, for miR-672-5p, we observed downregulation in pre-diabetic condition as compared to high-glucose condition which was also reported in cardiomyocytes induced by phenylephrine, angiotensin II, and insulin-like growth factor 1 [56]. Further, our in silico analysis revealed that its target genes were enriched in insulin signaling (p value: 0.003; fold enrichment: 5.9) and adrenergic signaling (p value: 0.02; fold enrichment: 3.7) pathways both of which becomes unresponsive during cardiac failure [57]. Zhao et al. have concluded miR-532-3p to be involved in atherosclerotic plaque formation and suggested that it can be utilized for therapeutic purposes by regulating its expression [58]. Exosomal mir-672-5p has also been studied for therapeutic applications in spinal cord injury as it targets Caspase-1 signaling pathway [59]. Overall, these two miRNAs depict differential expression in pre-diabetes condition and change in their expression upon high glucose might play a critical role in regulating key molecular pathways of DCM.

Conclusion

In conclusion, our study has identified differential miRNA expression in cardiomyoblast under pre-diabetes and diabetes conditions as compared to normal healthy cells. Further, except for few miRNAs, we observed no significant change in the expression of miRNAs between different hyperglycemic conditions. However, we identified several miRNAs that were not reported in DCM or any cardiovascular pathology before and found to regulate critical molecular pathways involved in DCM. We also identified and validated miR-532-3p and miR-672-5p depicting differential expression between pre-diabetes and diabetes along with probable role

in DCM. Therefore, further investigation of these miRNAs including target validation using higher DCM model must be performed in order to establish them as robust miRNAs biomarker and therapeutic molecule.

Supplementary Information The online version contains supplementary material available at https://doi.org/10.1007/s11010-022-04473-6.

Acknowledgements This work was supported by the research grant awarded to Prof. Vibha Rani by the Department of Science and Technology-Science and Engineering Research Board, Government of India (SERB File Number: EMR/2016/005914). We acknowledge Jaypee Institute of Information Technology (JIIT), for providing the infrastructural support. We would like to express our gratitude and appreciation to Dr. Sharad Saxena, Post-Doctoral fellow, ICGEB, Italy for invaluable assistance and suggestions for improvement.

Author contribution VR contributed to conceptualization, funding acquisition, project administration, resources, supervision, methodology, visualization, and writing, reviewing, and editing of the manuscript. PM contributed to data curation, formal analysis, investigation, software, validation and writing of the original draft.

Funding This work was supported by the Department of Science and Technology-Science and Engineering Research Board, Government of India (SERB File Number: EMR/2016/005914).

Data availability The datasets generated during and/or analyzed during the current study are available from the corresponding author on reasonable request.

Declarations

Conflict of interest There is no conflict of interest between the authors.

Ethical approval The study did not require any ethical approval.

References

1. International Diabetes Federation (2019) IDF diabetes atlas, 9th edn. Belgium, Brussels
2. Athithan L, Gulsin GS, McCann GP et al (2019) Diabetic cardiomyopathy: Pathophysiology, theories and evidence to date. World J Diabetes 10(10):490–510
3. Hippisley-Cox J, Coupland C (2016) Diabetes treatments and risk of heart failure, cardiovascular disease, and all cause mortality: cohort study in primary care. BMJ 354:i3477
4. Avogaro A, de Kreutzenberg SV, Negut C et al (2004) Diabetic cardiomyopathy: a metabolic perspective. Am J Cardiol 93(8):13–16
5. Rubler S, Dlugash J, Yuceoglu YZ et al (1972) New type of cardiomyopathy associated with diabetic glomerulosclerosis. Am J Cardiol 30(6):595–602
6. Trachanas K, Sideris S, Aggeli C et al (2014) Diabetic cardiomyopathy: from pathophysiology to treatment. Hell J Cardiol 55(5):411–421
7. Boudina S, Abel ED (2010) Diabetic cardiomyopathy, causes and effects. Rev Endocr Metab Disord 11(1):31–39
8. Shah AS, Gao Z, Urbina EM et al (2014) Prediabetes: the effects on rterial thickness and stiffness in obese youth. J Clin Endocrinol Metab 99(3):1037
9. Tian L, Zhu J, Liu L et al (2014) Prediabetes and short-term outcomes in nondiabetic patients after acute ST-elevation myocardial infarction. Cardiology 127(1):55–61
10. Erdogan D, Yucel H, Uysal BA et al (2013) Effects of pre-diabetes and diabetes on left ventricular and coronary microvascular functions. Metabolism 62(8):1123–1130
11. Saxena S, Mathur P, Shukla V et al (2019) Differential expression of novel MicroRNAs from developing fetal heart of Gallus gallus domesticus implies a role in cardiac development. Mol Cell Biochem 462(1–2):157–165
12. Guo L, Sun B, Wu Q et al (2012) miRNA–miRNA interaction implicates for potential mutual regulatory pattern. Gene 511(2):187–194
13. Paugh SW, Coss DR, Bao J et al (2016) MicroRNAs form triplexes with double stranded DNA at sequence-specific binding sites; a eukaryotic mechanism via which microRNAs could directly alter gene expression. PLoS Comput Biol 12(2):e1004744
14. Saxena S, Gupta A, Shukla V et al (2018) Functional annotation of differentially expressed fetal cardiac microRNA targets: implication for microRNA-based cardiovascular therapeutics. 3 Biotech 8(12):494
15. Yu XY, Song YH, Geng YJ et al (2008) Glucose induces apoptosis of cardiomyocytes via microRNA-1 and IGF-1. Biochem Biophys Res Commun 376(3):548–552
16. Zhang Y, Huang XR, Wei LH et al (2014) miR-29b as a therapeutic agent for angiotensin II-induced cardiac fibrosis by targeting TGF-β/Smad3 signaling. Mol Ther 22(5):974–985
17. Zhao F, Li BO, Wei YZ et al (2013) MicroRNA-34a regulates high glucose-induced apoptosis in H9c2 cardiomyocytes. J Huazhong Univ Sci Technol—Med Sci 33(6):834–839
18. Kong L, Zhu J, Han W et al (2011) Significance of serum microRNAs in pre-diabetes and newly diagnosed type 2 diabetes: a clinical study. Acta Diabetol 48(1):61–69
19. Shen Y, Xu H, Pan X et al (2017) miR-34a and miR-125b are upregulated in peripheral blood mononuclear cells from patients with type 2 diabetes mellitus. Exp Ther Med 14(6):5589–5596
20. Costantino S, Paneni F, Lüscher TF et al (2016) MicroRNA profiling unveils hyperglycaemic memory in the diabetic heart. Eur Heart J 37(6):572–576
21. Mathur P, Rani V (2021) MicroRNAs: a critical regulator and a promising therapeutic and diagnostic molecule for diabetic cardiomyopathy. Curr Gene Ther. https://doi.org/10.2174/1566523221666210311111619
22. Atale N, Chakraborty M, Mohanty S et al (2013) Cardioprotective role of *Syzygium cumini* against glucose-induced oxidative stress in H9C2 cardiac myocytes. Cardiovasc Toxicol 13(3):278–289
23. Bär C, Chatterjee S, Falcão Pires I et al (2020) Non-coding RNAs: update on mechanisms and therapeutic targets from the ESC working groups of myocardial function and cellular biology of the heart. Cardiovasc Res 116(11):1805–1819
24. Vasu S, Kumano K, Darden CM et al (2019) MicroRNA signatures as future biomarkers for diagnosis of diabetes states. Cells 8(12):1533
25. Yerlikaya FH, Öz M (2019) Aberrant expression of miRNA profiles in high-fat and high-sucrose fed rats. Clin Nutr Exp 1(27):1–8
26. Watkins SJ, Borthwick GM, Arthur HM (2011) The H9C2 cell line and primary neonatal cardiomyocyte cells show similar hypertrophic responses in vitro. In Vitro Cell Dev Biol-Anim 47(2):125–131
27. American Diabetes Association (2014) Diagnosis and classification of diabetes mellitus. Diabetes Care 37(Supplement 1):S81-90

28. Feng B, Chen S, Chiu J et al (2008) Regulation of cardiomyocyte hypertrophy in diabetes at the transcriptional level. Am J Physiol-Endocrinol Metab 294(6):E1119–E1126
29. Yang F, Zhang L, Gao Z et al (2017) Exogenous H2S protects against diabetic cardiomyopathy by activating autophagy via the AMPK/mTOR pathway. Cell Physiol Biochem 43(3):1168–1187
30. Copier CU, León L, Fernández M et al (2017) Circulating miR-19b and miR-181b are potential biomarkers for diabetic cardiomyopathy. Sci Rep 7(1):1–1
31. de Gonzalo-Calvo D, Kenneweg F, Bang C et al (2016) Circulating long-non coding RNAs as biomarkers of left ventricular diastolic function and remodelling in patients with well-controlled type 2 diabetes. Sci Rep 6(1):1–2
32. Fang L, Ellims AH, Moore XL et al (2015) Circulating microRNAs as biomarkers for diffuse myocardial fibrosis in patients with hypertrophic cardiomyopathy. J Transl Med 13(1):1–2
33. Ucar A, Gupta SK, Fiedler J et al (2012) The miRNA-212/132 family regulates both cardiac hypertrophy and cardiomyocyte autophagy. Nat Commun 3(1):1–1
34. Xu D, Zhang X, Chen X et al (2020) Inhibition of miR-223 attenuates the NLRP3 inflammasome activation, fibrosis, and apoptosis in diabetic cardiomyopathy. Life Sci 1(256):117980
35. Zhou J, Zhu Y, Fan J (2020) 23-LB: overexpression of microRNA-16 derepresses the mitochondrial function to exacerbate cardiomyopathy in streptozotocin-induced diabetic mice. Diabetes. https://doi.org/10.2337/db20-23-LB
36. Chavali V, Tyagi SC, Mishra PK (2014) Differential expression of dicer, miRNAs, and inflammatory markers in diabetic Ins2+/− Akita hearts. Cell Biochem Biophys 68(1):25–35
37. Jeyabal P, Thandavarayan RA, Joladarashi D et al (2016) MicroRNA-9 inhibits hyperglycemia-induced pyroptosis in human ventricular cardiomyocytes by targeting ELAVL1. Biochem Biophys Res Commun 471(4):423–429
38. Wang Z, Wang Z, Gao L et al (2020) miR-222 inhibits cardiac fibrosis in diabetic mice heart via regulating Wnt/β-catenin-mediated endothelium to mesenchymal transition. J Cell Physiol 235(3):2149–2160
39. Babu SS, Thandavarayan RA, Joladarashi D et al (2016) MicroRNA-126 overexpression rescues diabetes-induced impairment in efferocytosis of apoptotic cardiomyocytes. Sci Rep 6(1):1–2
40. Van Rooij E, Sutherland LB, Thatcher JE et al (2008) Dysregulation of microRNAs after myocardial infarction reveals a role of miR-29 in cardiac fibrosis. Proc Natl Acad Sci 105(35):13027–13032
41. Diao J, Cheng G, Zhao H et al (2021) Mir-148a attenuated oxidative stress in diabetic cardiomyopathy by negatively regulating crlreticulin. J Am Coll Cardiol 77(18_Supplement_1):650–650
42. Rawal S, Munasinghe PE, Nagesh PT et al (2017) Down-regulation of miR-15a/b accelerates fibrotic remodelling in the type 2 diabetic human and mouse heart. Clin Sci 131(9):847–863
43. Guedes EC, Franca GS, Lino CA et al (2016) MicroRNA expression signature is altered in the cardiac remodeling induced by high fat diets. J Cell Physiol 231(8):1771–1783
44. Li X, Du N, Zhang Q et al (2014) MicroRNA-30d regulates cardiomyocyte pyroptosis by directly targeting foxo3a in diabetic cardiomyopathy. Cell Death Dis 5(10):e1479–e1479
45. Huang DW, Sherman BT, Lempicki RA (2009) Systematic and integrative analysis of large gene lists using DAVID bioinformatics resources. Nat Protoc 4(1):44–57
46. Harris IS, Treskov I, Rowley MW et al (2004) G-protein signaling participates in the development of diabetic cardiomyopathy. Diabetes 53(12):3082–3090
47. Wu HE, Baumgardt SL, Fang J et al (2016) Cardiomyocyte GTP cyclohydrolase 1 protects the heart against diabetic cardiomyopathy. Sci Rep 6(1):1–4
48. Eguez L, Lee A, Chavez JA et al (2005) Full intracellular retention of GLUT4 requires AS160 Rab GTPase activating protein. Cell Metab 2(4):263–272
49. Larance M, Ramm G, Stöckli J et al (2005) Characterization of the role of the Rab GTPase-activating protein AS160 in insulin-regulated GLUT4 trafficking. J Biol Chem 280(45):37803–37813
50. Jiang X, Zhang JT, Chan HC (2012) Ion channels/transporters as epigenetic regulators?—a microRNA perspective. Sci China Life Sci 55(9):753–760
51. Choudhary G, Dudley SC Jr (2002) Heart failure, oxidative stress, and ion channel modulation. Congest Heart Fail 8(3):148–155
52. Saxena S, Jain A, Rani V (2017) MicroRNA-mediated MMP regulation: current diagnostic and therapeutic strategies for metabolic syndrome. Curr Gene Ther 17(3):214–227
53. Wang C, Zhao J, Nan X et al (2020) Long noncoding RNA CASC2 inhibits ox-LDL-mediated vascular smooth muscle cells proliferation and migration via the regulation of miR-532-3p/PAPD5. Mol Med 26(1):1–9
54. Chandrasekera DN, Neale JP, van Hout I et al (2020) Upregulation of microRNA-532 enhances cardiomyocyte apoptosis in the diabetic heart. Apoptosis 25:388–399
55. Kanaan Z, Roberts H, Eichenberger MR et al (2013) A plasma microRNA panel for detection of colorectal adenomas: a step toward more precise screening for colorectal cancer. Ann Surg 258(3):400–408
56. Lu Y, Wu F (2018) A new miRNA regulator, miR-672, reduces cardiac hypertrophy by inhibiting JUN expression. Gene 30(648):21–30
57. Lucia CD, Eguchi A, Koch WJ (2018) New insights in cardiac β-adrenergic signaling during heart failure and aging. Front Pharmacol 10(9):904
58. Zhao P, Wang Y, Zhang L, Zhang J, Liu N, Wang H (2021) Mechanism of long non-coding RNA metastasis-associated lung adenocarcinoma transcript 1 in lipid metabolism and inflammation in heart failure. Int J Mol Med 47(3):1
59. Zhou Z, Li C, Bao T, Zhao X, Xiong W, Luo C, Yin G, Fan J (2022) Exosome-shuttled miR-672–5p from anti-inflammatory microglia repair traumatic spinal cord injury by inhibiting AIM2/ASC/Caspase-1 signaling pathway mediated neuronal pyroptosis. J Neurotrauma. https://doi.org/10.1089/neu.2021.0464